AGE MODEL

Table of Annual Growth Rates

Growth rates for each annual pair of visible laminae (opaque-clear band couplets). The local hydrological year extends from the onset of the dry season (March) through the onset of precipitation in June and continued precipitation through February. Assuming that the base of each band couplet corresponds to early March, a linear fit across each annual layer gives an annual growth rate. The sampling frequency (number of stable isotope micro-samples per hydrological year) is also listed.

DATA, AGE MODEL & EXCURSIONS

Formatting

Although calcite samples were milled continuously, some samples were lost during sampling, sample preparation, or analysis.
Missing stable isotope data are reported as blank cells.

The base of each couplet of opaque-clear calcite is marked by a black lower border.
Each basal sample is defined in the age model (see above) as having been deposited in March of the corresponding year.

Data corresponding to the low $\delta^{18}O$ value excursions that we interpreted as cyclogenic are formatted in red.

Single-point change in $\delta^{18}O$ (or $\delta^{13}C$) value

Where data points are missing, change in stable isotope values are calculated from the last available data point.

Low $\delta^{18}O$ value excursions

Excursions are coded as 1, non-storm signal data are coded as 0.

Excursions were selected using a filter with the following rules:

1. If change in $\delta^{18}O$ value is positive, no excursion.
2. If change in $\delta^{18}O$ value is positive, and if the absolute value of change < 0.47 ‰, no excursion.
3. If change in δ^{13C} value is negative, and if the absolute value of change > 0.20 ‰, no excursion.

Also:

Low $\delta^{18}O$ value excursions cannot be associated with band edges to avoid the effects of any potential seasonal breaks in deposition.

Low $\delta^{18}O$ value excursions cannot be associated with the offset from a high $\delta^{18}0$ event.

Low $\delta^{18}O$ value Excursion Amplitude

The absolute value of the change in $\delta^{18}O$ value excursion size. For excursions with a two-point decline (e.g. 1993), the total change in $\delta^{18}O$ value is reported.

STATISTICAL ANALYSES

Data and Results are provided for statistical analyses of tropical cyclone frequency and intensity proxies.

Binary Logistic Regression model to discriminate cyclogenic excursions from background isotopic variability.

Standard Linear Regression models to test relations among stable isotope excursion amplitude, storm characteristics, and sampling frequency.

LIST OF APPENDICES

Appendix 1. Climate, Ecology, and Geologic Setting

Climate in Belize is tropical to subtropical. The average annual temperature in Central Belize is ~25 ˚C with about 1600 mm of annual rainfall (Frutos, 2006). Central Belize has a seasonal water deficit during the dry season (early March through late May), followed by summer monsoon rainfall (Fig. DR1). The wet season extends from June through January, transitioning to cold front precipitation by November. Precipitation is moderate in August during the so-called "little dry" period. Tropical cyclones have made landfall in Belize from June through November,

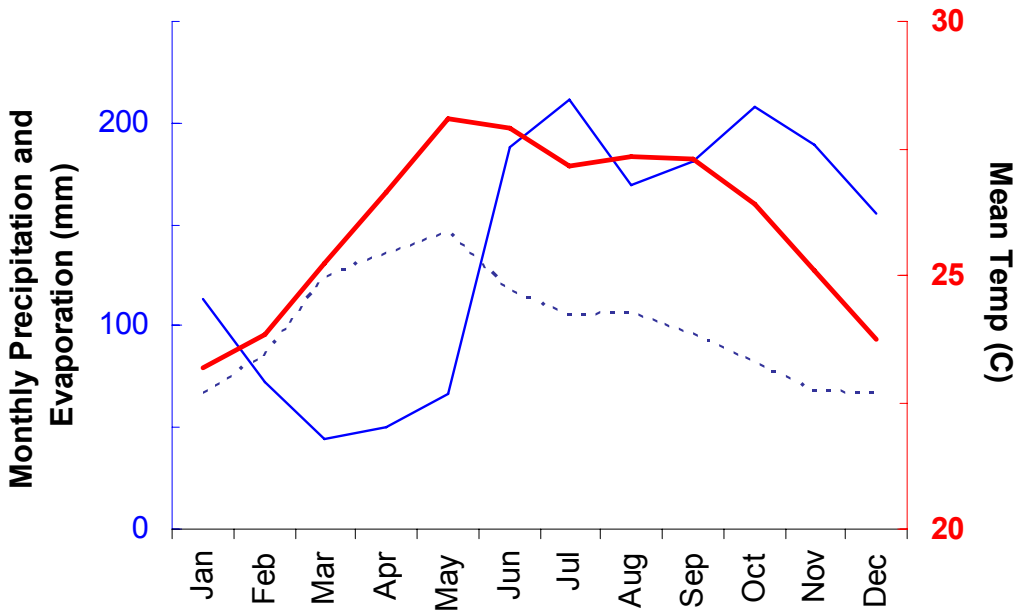

Figure DR1. Belize Climatology (Central Farm Meteorological Station, 1973-2005), including monthly precipitation (thin blue line), evaporation (dashed line), and mean temperature (bold red line). Water balance (precipitation – evaporation)is negative from February through May.

although September is the most active month (Fig. DR2) (Frutos, 2006). Tropical cyclone events are bracketed by other frontal and convective precipitation. Tropical cyclones bring heavy rainfall and flooding to Belize with a recurrence interval of ~2.5 years, contributing approximately 2.5% of annual precipitation (calculated for 1978 - 2001). Climate data is courtesy of the Belize Meteorological Service's Central Farm meteorological station, located less than 15 km from the field site. Between 1978 and 2000, Belize was affected by rainfall from 11 tropical cyclones. These storms varied in their maximum intensity prior to landfall, proximity to the cave site, and local precipitation amount (Table DR1).

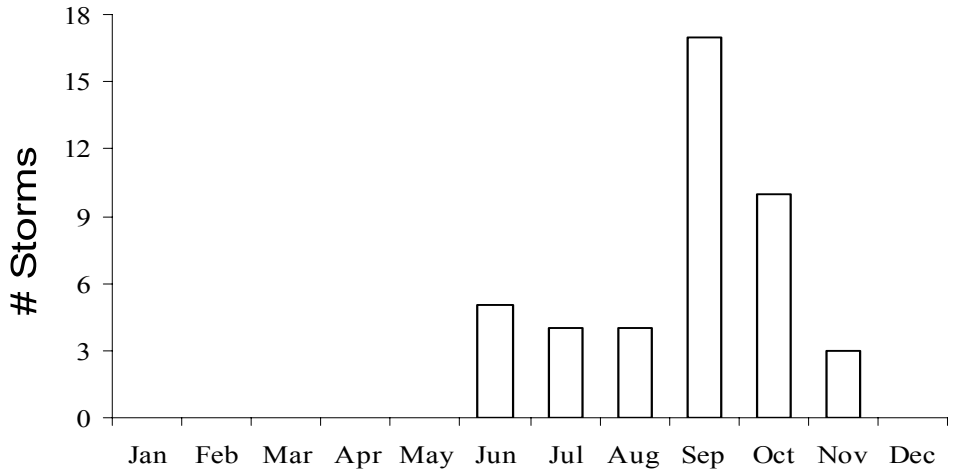

Figure DR2. Seasonality of Belize Hurricanes (1883 – 2005).
After Frutos, 2006. Tropical cyclones occur in the middle of the wet season.

TABLE DR1. RECENT TROPICAL CYCLONES NEAR CENTRAL BELIZE

Storm	Landfall date	Intensity *	Distance between storm track and cave (km)	Storm precipitation (mm) †
Keith	Oct. 2000	4	120	264
Katrina	Oct. 1999	0	158	15
Mitch 2	Nov. 1998	0	369	§
Mitch	Oct. 1998	5	282	246 §
Kyle	Oct. 1996	0	147	59
Dolly	Aug. 1996	1	233	51
Roxanne	Oct. 1995	3	311	43
Opal	Sep. 1995	0	248	68
Gert	Sep. 1993	0	86	24
Diana	Aug. 1990	0	259	24
Hermine	Sep. 1980	0	138	131
Greta	Sep. 1978	4	42	179

* Historical intensity, precipitation, and best track data for Atlantic tropical cyclones (NOAA Tropical Prediction Center). Intensity categories represent the maximum intensity at or prior to landfall in Central America, such that 0 indicates tropical storms, and values 1–5 indicate Saffir-Simpson hurricane intensity categories 1–5.

† Total rainfall during storm days is reported from the Central Farm meteorological station, less than 15 km from the cave.

§ Combined rainfall from both Hurricane Mitch landfall events.

Located between true rainforest of Southern Belize and the Yucatan tropical scrub to the north, the dominant forest type at the site is mature subtropical moist semi-evergreen broadleaf forest (Vreugdenhil et al. 2002). The cave is located in the Tapir Mountain Nature Reserve, which was donated to the Belizean government in 1975 and formally designated as a preserve in 1986. Common tree species include *Swietenia macrophilla* (mahogany), *Manilkara zapota* (chicle), *Brosimum alicastrum* (Ramon breadnut), *Orbigyna cohune* (cohune palm), *Cryosophila stauracantha* ("Give-and-Take Palm"), *Agonandra sp.*(guinweo vine), *Ficus crassiuscula* (strangling fig), *Cedrela odorata* (Spanish "cedar").

Limestones and dolomites of Late Cretaceous age and Paleozoic limestones make up the bulk of local bedrock (Miller, 1996). The cave site used in this study, Actun Tunichil Muknal (ATM), is developed in a massive pink limestone breccia. This bedrock unit correlates with a locally described rock unit in Central Belize known as the Albion formation or "Teakettle Diamictite," which has been identified as the K-T boundary in central Belize (King, 1996, Pope and Ocampo, 2000). This breccia unit, common in the Boundary Fault Karst region of Belize, has low primary porosity with major speleogenesis occurring in conjunction with fractures (Miller, 1996).

ATM is an active, multi-level phreatic cave with an underground river flowing through low passages (Miller, 1990). The river enters ATM through a sink in a different surface drainage basin, flowing underground for 5 km and ultimately emptying into Roaring Creek about 100 m from the resurgence. The keyhole-shaped active lower cave entrance at the resurgence shows clear geomorphic evidence of the downcutting origin of multiple upper-level passages. Elevated cave passages in ATM are heavily decorated with speleothems, and were used for ceremonial purposes by the Maya civilization c. 400-900 CE (Miller, 1990). Some speleothems are actively forming, while others appear desiccated. An upper level passage, about 500 m from the cave entrance, where speleothems were collected for this study has a stable temperature of 25°C and relative humidity of >90%. Bedrock overburden above this portion of the cave is at least 20 m in thickness, but may extend several tens of meters. Soil cores taken on the hill above the cave yielded thin, clay-rich soils (5-30 cm depth) with a minimal organic horizon and a thin covering of leaf litter. Carbonate bedrock outcrops also attest to the thin upland soils over ATM.

Appendix 2. Micro-Milling and Stable Isotope Analysis

Micro-samples were milled continuously from the polished surface of the ATM7 stalagmite slab at 20 μm intervals (Fig. 2) with a CM-1 micro-milling system custom-built by one of the authors (Carpenter). The system combines a fixed drill (Brasseler UP 200 controller and a UG 12 handpiece fitted with a 0.3 mm tungsten carbide dental bur), computer-controlled stage, and observation under a Nikon SMZU microscope. The CM-1 device specs are available from Carpenter Microsystems at http://www.microsampler.com. A rotational stage allowed us to rotate the sample relative to the drilling axis as milling progressed in order to maintain alignment with the growth axis (Fig. 2).

The width of the continuously-milled micromilling track is shown as a blue outline in Fig. 2. The depth of all micro- samples from the surface of the slab was approximately 0.5 mm. The first 37 samples (two annual layers in the uppermost 1.48 mm) were milled at 40 micron intervals, and 5-6 mm in width. It was clear at this point that a smaller drilling track would generate sufficient material for stable isotope analysis. The remaining micro-samples were milled at 20 micron intervals, where the track was approximately 2.5 mm in width. Individual calcite powder samples were transferred using a stainless steel scalpel from the milled surface to individual stainless steel-sample containers. Static electricity enables the calcite powder to cling to the scalpel so that powdered samples can be recovered reliably. Between samples, the drill bit and milling surface were cleaned with a stream of compressed air. Each 20 micron micro-sample represents one to several weeks of deposition. Some commercially available micro-milling equipment can be used to the same effect.

Stable Isotope Analysis was performed at the Paul H. Nelson Stable Isotope Laboratory at University of Iowa. Calcite powders were roasted *in vacuo* at 380ºC for one hour to remove volatile contaminants and then desiccated. We analyzed ~1300 samples using a Finnigan-MAT 252 IRMS with a Kiel III automated carbonate device. Powdered calcite samples (approximately 0.02 to 0.05 mg of $CaCO_3$ for each sample) were reacted with 2 drops of anhydrous phosphoric acid at 75ºC. Daily analysis of NIST powdered carbonate standards (NBS-18, 19, 20) and several in-house standards were conducted. Analytical precision on these standards was better than ±0.1 ‰ for both $\delta^{18}O$ and $\delta^{13}C$ values. All results are reported in per mil (‰) relative to V-PDB.

Appendix 3. Age Model

We have updated the age model initially published for this stalagmite record to correct counting errors in the originally published dataset. We show that these counting errors are related to the direct hydrological effects of heavy tropical cyclone precipitation. It is important to note that while the low $\delta^{18}O$ excursions were important in identifying counting errors, the stable isotope excursions themselves are not used as a dating tool. We avoid a circular argument for dating the low $\delta^{18}O$ excursions by using independent lines of evidence to test the updated age model, as outlined below. Thus verified, the updated age model can be used to determine the year in which low $\delta^{18}O$ excursions were deposited and compare those dates with the historical record of tropical cyclone activity in the area. In this section, we describe the initial age model development and justify the changes in the present work.

Major groundwater flushing events can result in double bands or couplets of speleothem calcite, representing a single annual period (e.g. Asmerom and Polyak, 2004 and references therein; Kaufmann and Dreybrodt, 2004; Proctor et al., 2000; Baker et al., 1993). Seasonal variations in drip rate or dripwater chemistry can result in regular changes in speleothem opacity, color, mineral fabric, or fluorescence. Central Belize experiences an annual water deficit from March through May followed by onset of the summer monsoon (Fig. DR1), conditions amenable to generating annual variations in dripwater chemistry and calcite morphology. The initial and updated age models are based on our interpretation of visible band pairs as annual deposits. After describing age model development and changes below, we show that both age models are supported by ^{137}Cs dating, and that the updated age model is further supported by independent stratigraphic, isotopic, and trace element evidence.

Radiometric Dating - The ^{137}Cs activity depth profile was used to test whether layer counting was consistent with an annual pattern of calcite deposition. Although no classical radioactive decay curve is evident in this dataset (e.g. Baskaran and Iliffe, 1993), the onset of ^{137}Cs activity is clearly demarcated (Fig. DR3). It is important to note that a classical decay curve is not necessarily predicted in this depositional setting. Cesium substitutes strongly for the macronutrient Potassium; as a result, in tropical ecosystems ^{137}Cs is not simply transmitted to the cave but is tightly cycled within the overlying ecosystem and soil (Ritchie and McHenry, 1990; Dörr and Münnich, 1989; Walker et al, 1997; Robison et al, 1997). However, the depth of ^{137}Cs activity onset provides sufficient age control to test the presence or absence of annual banding in this stalagmite. Using this approach, the error in ^{137}Cs dating is primarily related to the spatial resolution of ^{137}Cs samples and the assumptions used to derive ages from the depth of ^{137}Cs activity onset.

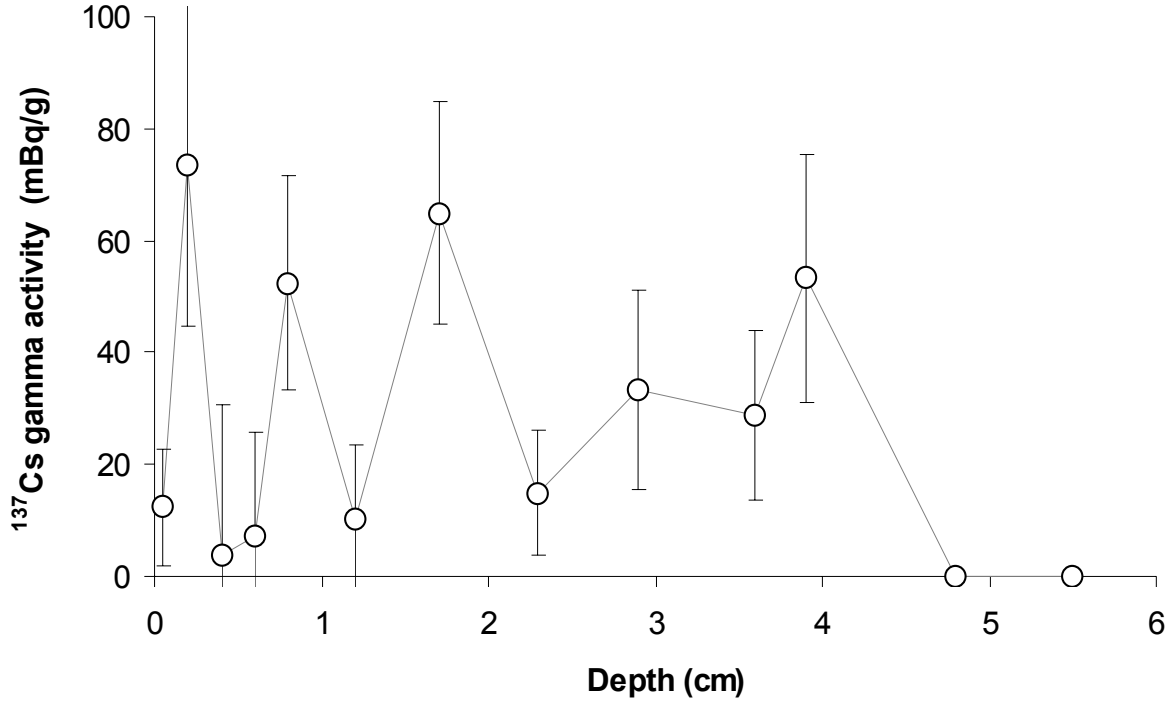

Figure DR3. ATM7 ^{137}Cs activity profile. Error bars are 1 standard deviation. Note that the activity of ^{137}Cs reaches zero below 3.9 mm.

The onset of ^{137}Cs activity at a depth between 48 mm and 39 mm marks the start of global atmospheric fallout from thermonuclear weapons testing (Shimada et al., 1996; Fig. A3). Because ^{137}Cs activity is only considered in a binary sense (detectable/undetectable), error in the following age estimates arise only from limitations in age bracketing from the spacing of calcite samples. We bracketed growth rates for the upper portion of ATM7 with three different assumptions:

1. The highest point at which zero ^{137}Cs activity was measured (-48 mm) reflects pre-atmospheric weapons testing conditions that prevailed in 1953 or earlier. This assumption yields a maximum growth rate of 1.02 $mm \cdot yr^{-1}$.
2. The depth of ^{137}Cs activity onset (-39 mm) may represent the onset of atmospheric fallout as early as 1954. This assumption yields a minimum growth rate of 0.85 $mm \cdot yr^{-1}$.
3. An early maximum of ^{137}Cs activity (-39 mm) may also represent the peak of thermonuclear fallout in 1963. This assumption yields a growth rate of 1.05 $mm \cdot yr^{-1}$.

The average of these three radiometrically-constrained growth rates was 1.03 $mm \cdot yr^{-1} \pm 0.08$.

Layer Counting and Initial Age Model - Paired visible couplets of clear and opaque calcite laminae in ATM7 are thought to correspond to the dry and wet seasons during the March – February hydrological year in central Belize (Frappier et al., 2002). The average radiometrically constrained growth rate estimate for the upper 60 mm (1.03 $mm \cdot yr^{-1} \pm 0.08$) was indistinguishable from the layer-counting growth rate calculated for the same section (1.04 $mm \cdot yr^{-1}$). However, we observed that layer thickness was greater in the upper ~two dozen couplets, the portion of ATM7 subjected to high-resolution stable isotope analysis (Fig. 2). We surmised that the growth rate was higher than average in the uppermost portion of ATM7. The layer-counting-based growth rate in the micro-sampled portion was slightly higher, 1.15 $mm \cdot yr^{-1}$. It seems that growth rates for both the radiometric technique and the more detailed annual layer-counting-based age model are thus consistent.

Having established consistency between ATM7 stratigraphic patterns and ^{137}Cs dating, we assumed that opaque-clear couplets are annual in nature. We assigned a linear growth function to each annual couplet to generate a refined age model with a March date for the base of each hydrological year (Frappier et al. 2002). In the absence of counting errors, the simplifying assumption of linear growth within each hydrological year results in variable dating error for individual stable isotope samples on the order of a few weeks to a few months.

Age Model Changes - However, we did identify counting errors in the original age model through recognition of stratigraphic associations between a few visible layers and tropical cyclone-related $\delta^{18}O$ value excursions. In addition to annual banding generated by strong seasonal water balance variations, smaller rainfall events could likewise perturb drip rates and calcite morphology. In fact, we observed many minor fluctuations in opacity *within* the clear portions of annual band couplets. Annual layer counting was not affected by most lesser rainfall events, which apparently do not perturb speleothem growth extensively enough to cause confusion with annual layers. However, infiltration from particularly intense rain events (e.g. Hurricane Keith, which produced over 26 cm of rain) would rapidly raise the hydraulic head of the drip water source conduit. The resulting sudden change in drip rate could temporarily perturb speleothem deposition to a greater degree than more frequent but smaller storms. *It is important to note that in the case of a major precipitation event, drip rate in the cave would be affected immediately upon stormwater infiltration, but water isotopic composition at the*

speleothem surface would not reflect the storm event until after enough time had passed to allow the isotopically-distinct stormwater to infiltrate from the surface to the cave site. Thus, we expected any physical changes in crystal opacity resulting from tropical cyclone precipitation to occur stratigraphically below any measured cyclogenic stable isotopic excursions.

In ATM7, one visible couplet that we originally classified as annual was deposited a few months before stalagmite collection, about the time that major Hurricane Keith struck Belize. We originally classified three additional visible couplets as annual deposits that we later found to be located stratigraphically below associated low $\delta^{18}O$ value excursions. On further examination, compared to other band pairs that we classified as annual, these four low $\delta^{18}O$ value excursion-related layers, or "storm couplets" were more akin to the minor sub-annual opacity variations than to other annual band pairs: storm couplets were typically much thinner, less distinct, and morphologically rougher and more angular. In the present work, we now recognize these storm couplets as sub-annual events generated by tropical cyclone rainfall rather than complete annual periods. Although weak fluctuations in opacity were also associated with other low $\delta^{18}O$ value excursions, apparently, most tropical cyclone precipitation events and other major storms did not affect speleothem stratigraphy enough to affect the initial layer-recognition and counting processes. Importantly, the high-resolution stable isotope record enabled us to distinguish clearly between the few cyclogenic storm couplets and annual couplets within the visible banding pattern. This discovery enabled us to refine the annual layer counting in the age model used in our previous analysis of this stalagmite (Frappier et al., 2002).

After accounting for the storm couplets, we re-assigned a linear growth function to each annual couplet as before to generate an updated age model with a March date for the base of each hydrological year (Fig. 2). The storm couplet at the top of the stalagmite (presumably generated by stormwater from Hurricane Keith) shifted the entire record forward by several months, and three older layers associated with low $\delta^{18}O$ value excursions (1990, 1980, and 1978) further shifted the lower part of the record.

Tests of the Updated Age Model - When plotted using the updated age model, ATM7 stable isotope, stratigraphic, and trace element variations are very consistent with regional climatology and local meteorological observations. Three lines of evidence validate the updated age model:

1. The ENSO teleconnection correlation previously identified in ATM7 (Frappier et al. 2002) remains robust and stable in the updated age model (Fig. 3). Previously, we showed a total correlation offset (or proxy record lag) between the ATM7 stable isotope record and the SOI of approximately 1.5 years (Frappier et al. 2002). This lag has two components, comprised of the teleconnection time (time between changes in the core ENSO region of the equatorial Pacific and subsequent changes in Belize), plus an infiltration or recharge component (time for meteoric water to percolate through the epikarst to the stalagmite surface). We now infer that the teleconnection lag component is approximately 1 year, based on studies showing that Caribbean weather responds to ENSO forcing after a lag of approximately one year (Tourre and White, 1995; 2005).

While we have not yet been able to conduct a long-term tracer test to quantify the exact timescale of recharge, additional information enables us to bracket the infiltration time to 3-6 months. Assuming that both components of the lag are stationary, the remainder of the correlation offset between the SOI and ATM7 stable isotope record (~0.5 years) also enables us

to estimate the percolation portion of the total time lag at approximately 6 months. The updated age model gives dates for each low $\delta^{18}O$ value excursion in the ATM7 record that match years of local tropical cyclone activity (Fig. 3). Another constraint comes from the lack of observation of any excursion from Hurricane Keith, which struck Belize just three months before the stalagmite was collected in Januray 2001. Given the excellent fidelity of the proxy record to earlier tropical cyclone events, we surmise that cyclogenic water from Hurricane Keith remained stored in the epikarst at the time of collection, and the infiltration time must be at least 3 months. An infiltration time of 3-6 months is reasonable for this site, and is consistent with the duration of the stratigraphic offset between storm couplets and associated low $\delta^{18}O$ value excursions. The consistency between the ATM7 record, 1-year regional teleconnection lag, and infiltration time estimate, combined with the stability and clarity of the ENSO correlation together provide good evidence that the updated age model is correct.

2. The extended low $\delta^{18}O$ value interval near the base of the ATM7 record (located between K and J in Fig. 3) now dates to 1979, a year when local precipitation exceeded 2856 mm, more than three standard deviations (1σ = 323 mm·yr^{-1}) above the climatological average (1618 mm·yr^{-1}). This extended period of low $\delta^{18}O$ values is thus an expression of the "amount effect" and is unrelated to tropical cyclone precipitation events (Rozanski et al., 1997). Visible stratigraphy also reflects the extreme wetness of 1979. A distinct, rusty-colored layer apparent in the polished cross-section (Fig. 2) and trace element event (described below) is embedded within this extended period of low $\delta^{18}O$ values. This isotopic, trace element, and stratigraphic horizon constitutes an event horizon that is best explained by the combined effects of the extremely wet weather conditions that prevailed in central Belize during 1979.

3. Two different, major trace element perturbations in this stalagmite are dated to 1979 and 1982 using the updated age model (Frappier, 2006). The 1979 trace element event corresponds to the wet year and associated stratigraphic and isotopic changes in the ATM7 record described above. The 1982 trace element event represents an even greater disruption of the site's biogeochemistry, and is unique in record (2001 – 1978). The 1982 trace element event is significant because it occurred in a year when clouds of tephra from the eruption of the El Chichon volcano in nearby Chiapas, Mexico were observed to cover the study area. This 1982 trace element event thus constitutes a marker horizon of known age that confirms the validity of the ATM7 age model update presented here.

Together, these three independent and consistent lines of evidence provide a rigorous test of the updated age model. Isotopic, stratigraphic, and trace element evidence consistently support the updated age model, enabling us to avoid the circular use of the low $\delta^{18}O$ value excursions to date the stalagmite itself. The excellent temporal match observed between the history of storm events in this area and low $\delta^{18}O$ value excursions in ATM7 is thus an application of the updated age model, and not a support for that age model. The remaining age model error is related to the assumption of linear deposition within each annual couplet, indicating dating uncertainty for individual stable isotope samples of a few weeks to a few months.

Appendix 4. Paleo-Hurricane Intensity Proxy Analysis

To investigate the relations between signal amplitude and storm characteristics, we performed a standard multiple linear regression for the eleven storm signals we identified as cyclogenic. The four independent variables were storm maximum intensity at or prior to landfall (integer Saffir-Simpson intensity categories, Table 1) (*I*), minimum distance between storm track and cave site (km) (*D*), mean storm precipitation recorded at three nearby meteorological stations (mm) (*P*), and sampling frequency (number of micro-samples per year) (*S*). Input data can be found in the accompanying Excel database.

Sampling frequency could exert a strong control on the ability of this technique to resolve the isotopic signature from very brief individual storm infiltration events. Given a constant sampling interval of 20 μm, inter-annual and sub-annual variations in stalagmite growth rate would control extent of contamination in storm micro-samples by adjacent, isotopically "normal" background calcite. Although seasonal growth rate variations may be large, the tropical cyclone events in this dataset all occur within the rainy season (Fig. DR2). Thus, sampling frequency is likely to be relatively stable for different storm events occurring within the same season. For multiple tropical cyclones in the same year, the measured amplitude of excursions is more likely to be controlled by differences in precipitation $\delta^{18}O$ values. In contrast, growth rate differences *between* years has a relatively large effect on the amount of time represented by each sample, and thus could substantially affect the measured amplitude of different cyclogenic excursions. The parameter sampling frequency varies with annual growth rate, but remains constant for multiple storm strikes during a single year, in keeping with our understanding of the relations among sampling, growth rate, and measured excursion amplitude. For example, within each of the multiple strike years 1995 and 1996, *S* (sampling frequency) was stable and more intense storms were associated with larger excursions (Fig. 3). Between these two years, larger excursions were measured in the year with higher sampling frequency (1996) (Fig. 3).

The overall regression model results (Adj. R^2= 0.654, p=0.030) are explained in Results, and tabulated below (Table A1). Distance to storm track was not a significant contributor to the overall model, and was not correlated with any other independent variables. Not surprisingly,

TABLE DR2. RESULTS OF A MULTIPLE LINEAR REGRESSION TO INVESTIGATE STORM AND SPELEOTHEM FACTORS RELATED TO THE SIGNAL SIZE OF MEASURED $\delta^{18}O$ VALUE EXCURSIONS.

Factor	Coefficients		correlations		tolerance	sig.
	unstandard-ized	Standard-ized	zero-order	semi-partial		
Constant	0.353	n/a	n/a	n/a	n/a	0.182
Maximum Intensity	0.240	1.266	0.582	0.593	0.219	0.019
Resolution (samples/ yr)	0.007	0.662	0.388	0.619	0.874	0.016
Distance to Storm Track (km)	0.001	0.182	0.247	0.170	0.877	0.395
Local Precipitation (mm)	-0.003	-0.643	0.383	-0.305	0.225	0.152

local rainfall was highly correlated with storm maximum intensity. The correlation between storm maximum intensity and local precipitation means that reconstructions of past storm intensity also closely reflect the amount of local precipitation generated by those storm events. Interestingly, local storm precipitation is not significantly correlated with $\delta^{18}O$ signal size, suggesting that given sufficient sampling resolution $\delta^{18}O$ signal size is controlled substantially by the maximum intensity reached by the tropical cyclone while producing rainfall at the cave site, and is not a simple, direct expression of the local "amount effect".

References Cited

Asmerom, Y., and Polyak, V. J., 2004, Comment on Betancourt et al. (2002) ''A test of annual resolution in stalagmites using tree rings'': Quaternary Research, v. 61, p. 119-121.

Baker, A., Smart, P. L., Edwards, R. L., and Richards, D. A., 1993, Annual Banding in a Cave Stalagmite: Nature, v. 364, p. 518-520.

Baskaran, M. and T. M. Iliffe, 1993. Age determination of recent cave deposits using excess 210-Pb - A new technique. Geophysical Research Letters 20(7): 603-606.

Carpenter, S.J., 1996, A new microsampling device for extracting high-resolution isotope data from geologic and biologic materials: Geological Society of *America Abstracts with Programs*, p. 360. Further details available at http://www.microsampler.com/

Dörr, H. and Münnich, K. O., 1989, Downward movement of soil organic matter and its influence on trace-element transport (^{210}Pb, ^{137}Cs) in the soil. Radiocarbon 31(3):655-663.

Frappier, A. B., 2006. Empirical orthogonal function analysis of multivariate stalagmite trace element data: Detecting the 1982 El Chichón volcanic eruption. In: *Archives of Climate Change in Karst,* Karst Waters Institute Special Publication 10, p. 113-115. Proceedings of the symposium Climate Change: The Karst Record (IV), 26-29 May, 2006, Baile Herculane, Romania.

Frutos, R. 2006. The Climate of Belize, http://www.hydromet.gov.bz/ March 2, 2006

Vreugdenhil, D., J. Meerman, A. Meyrat, L. Diego Gómez, and D. J. Graham. 2002. Map of the Ecosystems of Central America: Final Report. World Bank, Washington, D.C.

Kaufmann, G., and Dreybrodt, W., 2004, Stalagmite growth and palaeo-climate: an inverse approach: Earth and Planetary Science Letters, v. 224, p. 529-545.

King, D. T. Jr., 1996, Cayo District Cretaceous-Tertiary boundary stratigraphy, Belize. Planetary Report, v. 16, p. 10-11. http://www.auburn.edu/~kingdat/kt_boundary_page.htm#two

Lawrence, J. R., Gedzelman, S. D., Zhang, X. P., and Arnold, R., 1998, Stable isotope ratios of rain and vapor in 1995 hurricanes: Journal of Geophysical Research-Atmospheres, v. 103, p. 11381-11400.

Miller, T., 1990. Belize: Tunichil Muknal. National Speleological Society News 48(2): 32-35.

Pope, K.O., and A.C. Ocampo, 2000, Chicxulub high-altitude ballistic ejecta from central Belize: Lunar and Planetary Science, v. 31, n. 1419.

Proctor, C. J., Baker, A., Barnes, W. L., and Gilmour, R. A., 2000, A thousand year speleothem proxy record of North Atlantic climate from Scotland: Climate Dynamics, v. 16:815-820.

Ritchie and McHenry, 1990. Application of radioactive fallout cesium-137 for measuring soil erosion and sediment accumulation rates and patterns: A review. Journal of Environmental Quality, v. 19: 215-233.

Robison, W. L., C. L. Conrado, And T. F. Hamilton, 1997. A comparative study on 137Cs transfer from soil to vegetation in the Marshall Islands, International Meeting on Influence of Climatic Characteristics upon Behavior of Radioactive Elements, October 14–16, 1997, Aomori, Japan.

Rozanski, K., Johnsen, S. J., Schotterer, U., and Thompson, L. G., 1997, Reconstruction of past climates from stable isotope records of palaeo-precipitation preserved in continental archives: Hydrological Sci. Journal, v. 42, p. 725-745.

Tourre, Y.M., and White, W.B., 2005. Evolution of the ENSO signal over the tropical Pacific-Atlantic domain Source: Geophysical Research Letters, v.32, n.7, L07605, doi:10.1029/2004GL022128,

Tourre, Y.M., and White, W.B., 1995. ENSO Signals In Global Upper-Ocean Temperature Source: Journal of Physical Oceanography, v. 25, n. 6, p. 1317 -1332.

Walker, R.; Gessel, S.; Held, E., 1997. The ecosystem study on Rongelap Atoll. Health Physics, 73(1): 223-233.